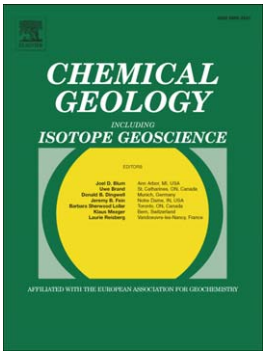


# Complexation of Zr and Hf monomers in supercritical aqueous solutions: Insights from *ab initio* molecular dynamics simulations

Sandro Jahn, Julien Dubrail, Max Wilke

PII: S0009-2541(14)00452-5
DOI: doi: 10.1016/j.chemgeo.2014.10.012
Reference: CHEMGE 17377

To appear in: *Chemical Geology*

Accepted date: 16 October 2014

# Complexation of Zr and Hf monomers in supercritical aqueous solutions: Insights from *ab initio* molecular dynamics simulations

Sandro Jahn[a,*], Julien Dubrail[a], Max Wilke[a]

[a] *GFZ German Research Centre for Geosciences, Section 3.3, Telegrafenberg, 14473 Potsdam, Germany*

**Abstract**

The enhanced mobilization of high field strength elements (HFSE) by certain geological fluids at high pressures, $P$, and high temperatures, $T$, as indicated by field observations and recent solubility measurements is most likely related to the type of complex formation in the fluid phase. However, only a few *in situ* experimental studies have been performed so far to constrain HFSE speciation in supercritical aqueous fluids. Here, we complement these investigations by *ab initio* molecular dynamics simulations to explore the complexation of $Zr^{4+}$ and $Hf^{4+}$ monomers in aqueous solutions at $T = 1000$ K and $P \sim 1$ GPa. Regardless of the type of fluid (basic, neutral, acidic) both Zr and Hf seem to prefer an octahedral coordination. By systematically changing fluid composition and coordinating anions, the structure of various $[(Zr,Hf)Cl_k(OH)_m(H_2O)_n]^{4-k-m}$ ($k = 0-6$, $m = 2-6$, $n = 0-4$) complexes is investigated. For each complex that is stable on the time scale of the simulation, theoretical X-ray absorption spectra are calculated and compared to experimental data. From this comparison, the most likely complexes in HCl solutions are $[(Zr,Hf)Cl_3(Cl,OH)_2(H_2O)]^-$. The differences between experimental and theoretical XANES spectra present in the case of NaOH solutions indicate HFSE speciation beyond monomers in this system. Charge-neutral $[(Zr,Hf)(OH)_4(H_2O)_{1-2}]$ complexes, which may be the dominant species in neutral fluids at very low HFSE concentrations, show the lowest coordination (5.2(1)) of all investigated species. Finally, differences in the complexation of Zr and Hf

*Preprint submitted to Chemical Geology* *September 26, 2014*

*Corresponding author. Tel.: +49 331 288 1483; fax: +49 331 288 1402.
*Email address:* jahn@gfz-potsdam.de (Sandro Jahn)

in aqueous solutions at ambient and supercritical conditions and the possible formation of more complex oligomeric species are discussed.

*Keywords:* ab initio molecular dynamics, high field strength element, aqueous solution, speciation, subduction zone

## 1. Introduction

High field strength elements (HFSE), i.e. Ti, Zr, Hf, Nb and Ta, are tracers of considerable importance for large-scale mass and energy transfer in the Earth's interior. This is particularly true for those processes occurring within subduction zones because they involve differential mobilization of elements producing the characteristic depletion of HFSE relative to large-ion-lithophile elements (LILE), i.e. Rb, Sr, Cs, Ba, Pb, U and Th, in primitive arc magmatism compared to mid-ocean ridge basalt (Perfit et al., 1980; McCulloch and Gamble, 1991; Elliot et al., 1997). The depletion of HFSE in arc magmas is usually assigned to preferential mobilization of LILE during fluid-release from the subducted slab, where HFSE strongly partition into accessory phases like zircon or rutile. Both phases are found in many lithologies and are stable over a wide pressure and temperature range. Thus, they largely control the distribution of HFSE during metamorphic and melting reactions. For example, when rutile or zircon are formed during fluid-rock interaction in metamorphic reactions this leads to retention of HFSE. This view assumes that the solubility of these phases is low in subduction zone fluids. The solubility of rutile and zircon in $H_2O$ is indeed very low as found by experiments at high pressure and temperature (Tole, 1985; Tropper and Manning, 2005; Audetat and Keppler, 2005; Newton et al., 2005, 2010; Bernini et al., 2013). While this model may explain the large-scale picture and the trace-element patterns of arc magmas, there is ample field evidence that both accessory phases may be mobilized during metamorphism: e.g. Ti-minerals in hydrothermal clefts of metamorphic rocks (Philippot and Selverstone, 1991; John et al., 2008) or examples of zircon with textures or structures that imply

dissolution and recrystallization, even in low-grade metamorphic rocks (Liati and Gebauer, 1999; Möller et al., 2002; Dempster et al., 2004). These observations seem to be in conflict with the explanation for the HFSE-depletion in arc magmas, which is based on the assumption of low solubility of these accessory phases in aqueous fluids. Thus, there is considerable need for a better understanding of the parameters controlling the solubility of HFSE-bearing minerals to provide a persisting model that may explain both, the large scale picture evidenced by arc-magmas and the one observed in metamorphic rock units.

The most substantial enhancement of the solubility was observed as a function of the aqueous fluid composition, i.e. in the presence of complexing agents. This is of major relevance, because pure water is not an adequate approximation for the composition of subduction zone fluids. In case of rutile, significant solubility increase was found for fluids containing dissolved $Cl^-$ or $F^-$ (Rapp et al., 2010) as well as alkali-aluminosilicate components (Manning et al., 2008; Antignano and Manning, 2008; Hayden and Manning, 2011). In case of zircon, there is similarly substantial solubility enhancement for acidic and basic solutions (Ewing et al., 1982; Tole, 1985; Aja et al., 1995; Schmidt et al., 2006; Kovalenko and Ryzhenko, 2009) or addition of NaCl (Bernini et al., 2013). Also for zircon, dissolution of alkali-aluminosilicate components in the fluids dramatically enhances the solubility (Wilke et al., 2012). The strong dependence of the solubility on the amount and type of dissolved silicate components provides an efficient way of controlling HFSE mobility in natural fluids, i.e. through the rock matrix, which buffers the composition of fluids in equilibrium within a given lithology.

The difference in solubility with fluid composition is likely driven by the difference in the complexation of HFSE in those fluids. At ambient and subcritical conditions, thermodynamic analysis of solubility has been used to derive insights to the speciation of Zr or Hf. For Zr, thermodynamic models usually assume charge neutral $[Zr(OH)_4](aq)$ monomeric species as the dominant complex in aqueous solution over a wide range of pH conditions (Aja et al., 1995; Veyland

et al., 1998; Ekberg et al., 2004; Qiu et al., 2009). At strongly basic conditions (pH > 10), additional OH groups are assumed to form $[Zr(OH)_5]^-$(aq) or $[Zr(OH)_6]^{2-}$(aq). Under strongly acidic conditions, the number of OH groups in the first coordination shell is reduced, in the extreme case to a fully hydrated $Zr^{4+}$(aq) ion. With increasing $F^-$ or $SO_4^{2-}$ activity, associated $[ZrF_x]^{(4-x)}$(aq) or $[Zr(SO_4)_x]^{(4-2x)}$(aq) species are described (Aja et al., 1995; Ryzhenko et al., 2008). More recently, evidence for mixed hydroxyfluoride complexes was found (Migdisov et al., 2011). Ekberg et al. (2004) suggest additional formation of $[Zr_4(OH)_8]^{8+}$(aq) and $[Zr_2(OH)_6]^{2+}$(aq) complexes at strongly acidic conditions. From solubility measurements using the undersaturation method, solubility product and hydrolysis constants were obtained assuming mononuclear $Zr^{4+}$(aq), $[ZrOH]^{3+}$(aq) and $[Zr(OH)_4]$(aq) species (Kobayashi et al., 2007).

At ambient conditions, extended x-ray absorption fine structure (EXAFS) measurements on $Zr^{4+}$ and $Hf^{4+}$ ions in acidic solution confirm polynuclear clusters as the predominant species in solutions with pH larger than zero and Zr or Hf concentrations larger than $10^{-4}$ mol/kg (Hagfeldt et al., 2004). Fully hydrated $Zr^{4+}$(aq) and $Hf^{4+}$(aq) were observed for pH lower than zero. From the bond length distribution it was concluded that the first hydration shell of the monomeric species contains eight or perhaps seven $H_2O$ molecules (Hagfeldt et al., 2004). A second shell attributed to Zr-Zr distances in polynuclear clusters was found in an EXAFS study of $Zr^{4+}$ in acidic solution (Cho et al., 2005). In basic solutions, the same group found evidence for $[Ca_3Zr(OH)_6]^{4+}$(aq) complexes (Brendebach et al., 2007). A thermodynamic equilibrium of tetrameric and octameric species in acidic aqueous solutions with 0.05 mol/kg $Zr^{4+}$ was concluded from small-angle x-ray scattering experiments (Singhal et al., 1996).

The speciation found at ambient conditions is not transferable to supercritical fluids at metamorphic conditions. Particularly, the highly charged species reported for aqueous solutions at very high or low pH, such as fully hydrated $[(Zr,Hf)(H_2O)_{6-8}]^{4+}$ or oligomeric species such as the tetramer $[Zr_4(OH)_8(H_2O)_{16}]^{8+}$

are not very likely due to the strongly decreased dielectric constant of the solvent (Weingärtner and Franck, 2005). Wilke et al. (2012, 2013) and Louvel et al. (2013) constrained the compositional dependence of Zr and Hf complexation in supercritical fluids by X-ray absorption near-edge structure (XANES). In Wilke et al. (2012, 2013), experimental information on the HFSE complexation was obtained for aqueous fluids with HCl, NaOH, $Na_2Si_3O_7$ (NS3), or $Na_2Si_3O_7$ + 1 or 5 wt% $Al_2O_3$, equilibrated with zircon or hafnon in hydrothermal diamond anvil cells at $T$ up to about 1000 K and $P$ up to about 1 GPa. *Ab initio* modeling of the XANES based on simple polyhedral clusters and comparison to experiment provided qualitative insight to the difference on the complexation. For NS3 ± $Al_2O_3$ solutions, measured XANES at the Zr-K and Hf-$L_3$ edges indicated complexes with six oxygens in the first shell. In contrast, seven oxygens are indicated in the NaOH solution. For 16 wt% HCl solutions, a spectrum simulated for a $(Zr,Hf)O_4Cl_3$ cluster reproduced qualitatively the features of the experimental spectra (Wilke et al., 2012). Louvel et al. (2013) confirmed the sixfold coordination of Zr in alkali silicate solutions. Using a less concentrated 2.5 wt% HCl solution they found no evidence for extensive Zr-Cl complexation in such fluids at supercritical conditions but discuss the possible presence of up to two Cl atoms in an assumed eight-fold Zr coordination shell.

*Ab initio* molecular dynamics (AIMD) simulations have become a powerful tool to model cation complexation in aqueous fluids in a wide range of pressures and temperatures (e.g. Jahn and Wunder (2009); Sherman (2010); Jahn and Schmidt (2010); Liu et al. (2012); Mei et al. (2013); Watenphul et al. (2014)). For Zr and Hf, previous computational studies were concerned with the stability of the $[Zr_4(OH)_8(H_2O)_{16}]^{8+}$ tetramer (Rao et al., 2007) or the fully hydrated $[(Zr,Hf)(H_2O)_{6-8}]^{4+}$ complex at ambient conditions (Messner et al., 2011b,a). In the study of Messner et al. (2011b), a hydrolysis reaction was observed at $T > 600$ K. Speciation of $Ti^{4+}$ in ambient and supercritical water was investigated by AIMD and metadynamics simulations (van Sijl et al., 2010, 2011). While the

most stable fully hydrated $Ti^{4+}$(aq) complex consisted of five hydration waters, six water ligands were observed at supercritical conditions.

Here, we present results of AIMD simulations of $Zr^{4+}$ and $Hf^{4+}$ monomers in aqueous solutions at supercritical conditions ($P \sim 1$ GPa and $T = 1000$ K). Changes in cation speciation for different solvents, including NaOH and HCl solutions as well as pure $H_2O$ fluid, are investigated. The main goals of this study are to explore the complexation of these important elements under well-defined conditions in simple model fluids and to relate the predicted molecular structure to experimental observations. For the latter, theoretical spectra of the x-ray absorption near-edge structure (XANES) are computed and compared to recent measurements (Wilke et al., 2012; Louvel et al., 2013). We consider this study a starting point for a systematic and comprehensive theoretical investigation of HFSE complexation in complex geological fluids.

## 2. Computational Method

### *2.1. Simulation cell setup*

In this study, the complexation of Zr and Hf monomers in alkaline, neutral and chlorine-bearing acidic solutions is explored. For choosing a feasible molecular modeling strategy one has to keep in mind that the ligand exchange for highly charged ions is rather slow on the timescale available to AIMD and that many first shell coordination environments with $H_2O$, $OH^-$, and $Cl^-$ ligands are possible. Therefore, we sample possible coordination environments of Zr and Hf in separate AIMD runs and compare their theoretical x-ray absorption spectra to experimental data. A summary of the investigated fluid compositions is compiled in Table 1.

In a first set of simulations we studied the behavior of initial $[Zr(OH)_n]^{4-n}$ and $[Hf(OH)_n]^{4-n}$ clusters with $n = 0$ to 8 in an aqueous environment consisting of 32 $H_2O$ molecules (Runs Hy0 to Hy8). This setup explores the complexation

Table 1: Compositions of the investigated solutions, simulation cell charge where different from zero, and cubic box length $a$. All simulations were run at $T = 1000$ K and a corresponding pressure of about 1 GPa.

| Run | Composition | charge | $a$ (Å) |
|---|---|---|---|
| #Hy0 | (Zr/Hf)+32 $H_2O$ | +4 | 10.16 |
| #Hy2 | (Zr/Hf)$(OH)_2$+32 $H_2O$ | +2 | 10.37 |
| #Hy4 | (Zr/Hf)$(OH)_4$+32 $H_2O$ | | 10.57 |
| #Hy6 | (Zr/Hf)$(OH)_6$+32 $H_2O$ | -2 | 10.76 |
| #Hy8 | (Zr/Hf)$(OH)_8$+32 $H_2O$ | -4 | 10.94 |
| #Na5 | (Zr/Hf)$(OH)_4$+32 $H_2O$+5 NaOH | | 11.13 |
| #Na6 | (Zr/Hf)$(OH)_4$+30 $H_2O$+6 NaOH | | 11.13 |
| #Cl6 | (Zr/Hf)$Cl_4$+35 $H_2O$+2 HCl | | 11.13 |
| #Cl7 | (Zr/Hf)$Cl_4$+34 $H_2O$+3 HCl | | 11.13 |
| #Cl9 | (Zr/Hf)$Cl_4$+32 $H_2O$+5 HCl | | 11.13 |

Zr or Hf monomers with a pure $H_2O$ or a mixed $H_2O$-OH hydration shell and excludes metal cations in the second coordination shell. The spatial dimensions of the cubic simulation cells were chosen to sample pressures of approximately 1 GPa at $T = 1000$ K according to the equation of state of pure water (Wagner and Pruss, 2002). Corresponding cell lengths ranged from 10.16 Å ($n = 0$) to 10.94 Å ($n = 8$). For those runs with charged initial complexes, a uniform background charge was used to ensure global charge neutrality.

We then modeled Zr and Hf complexation in a number of charge neutral fluids representing either basic NaOH or acidic HCl solutions. Aqueous NaOH solutions contained an initial $Zr(OH)_4$ or $Hf(OH)_4$ complex and either 30 $H_2O$ + 6 NaOH or 32 $H_2O$ + 5 NaOH. For the HCl solutions, different AIMD simulations were started with initial configurations containing zero to six Cl in the first coordination shell of Zr or Hf. Six different AIMD runs of type #Cl6 (#Cl6a to #Cl6f,

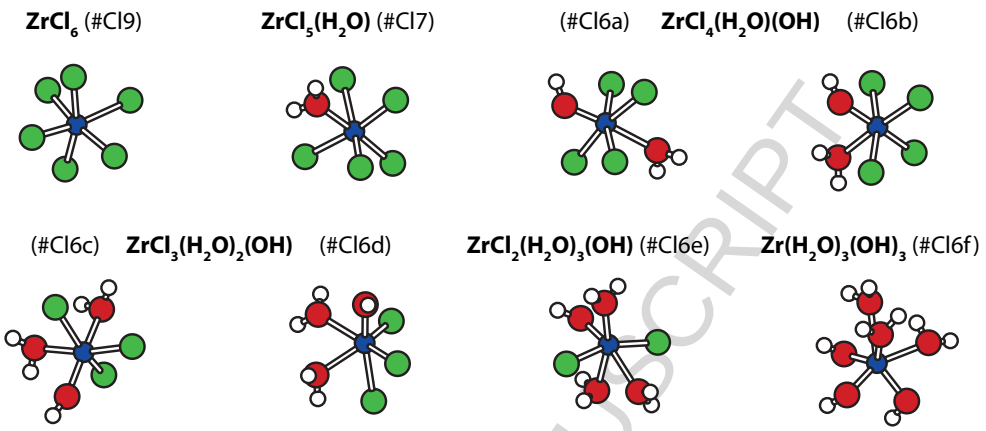


Figure 1: Snapshots of six-fold coordinated Zr (blue) complexes from different runs of the chloride solutions. Cl ligands are shown as green balls, OH and $H_2O$ as large red (O) and small white (H) balls. The corresponding runs of the Hf-bearing chloride solutions have the same arrangement of coordinating anions with exception of run #Cl6f where Hf is coordinated to one chlorine and five oxygen atoms.

see Table 1 and Fig. 1) were performed for both Zr and Hf to sample coordination environments in chloride fluids ranging from zero to four Cl. The evolution of (Zr,Hf)$Cl_5$ and (Zr,Hf)$Cl_6$ complexes in solution were studied in runs #Cl7 and #Cl9.

Some of the initial simulation cells were set up from scratch. In these cases, clusters containing a central Zr or Hf atom and a first coordination shell consisting of $H_2O$, $OH^-$ and/or $Cl^-$ ligands were surrounded by a number of randomly positioned $H_2O$ molecules representing the aqueous solution. Other starting configurations were derived from previous simulations by exchanging molecules from the first coordination shell of Zr or Hf with molecules in the solvent, e.g. by exchanging a $Cl^-$ ligand with an $H_2O$ or $OH^-$ molecule in the bulk solution. Some solutions of runs #Hy0 to #Hy8 were derived from previous runs by removing individual OH groups from the first hydration shell of Zr/Hf and adopting the cell volume and the charge-compensating background. At the conditions of the AIMD simulations (see below) hydrogen dynamics is fast and local charge equili-

bration is reached quickly within the first few picoseconds. Therefore, the initial simulation cell setup mainly determines the distribution of oxygen and chlorine atoms between the Zr/Hf nearest neighbor environment and the bulk solution. Since the simulation cells from the random structure approach are further away from equilibrium than those from the molecule exchange approach, they require longer times for equilibration. Otherwise, no significant dependence on the type of simulation cell setup could be observed. Two of the Zr solutions were also run with a larger simulation cell containing 59 $H_2O$ molecules to check possible finite size effects, but for the properties of interest here no discernible differences to the 32 $H_2O$ cells could be found.

### *2.2. Ab initio molecular dynamics simulations*

*Ab initio* molecular dynamics simulations were performed using the CPMD code (Marx and Hutter, 2000), which uses density-functional theory with a planewave basis set and pseudopotentials for the core electrons. The energy cutoff for the planewave was set to 80 Rydberg. The exchange-correlation energy was calculated using the generalized gradient approximation according to Perdew-Burke-Ernzerhof (Perdew et al., 1996). Temperature was controlled using a Nosé-Hoover thermostat (Nosé, 1984). All simulations were run at a constant temperature of 1000 K. A time step of 0.5 fs was chosen for the Born-Oppenheimer molecular dynamics simulations. Typical production trajectories were collected for at least 10 ps. All the calculations were performed using periodic boundary conditions.

Initially, we used the Martins-Troullier type pseudopotentials provided with the CPMD code for both Zr- and Hf-bearing solutions. However, the initial Hf pseudopotential did not contain semi-core electrons whereas that of Zr did. Comparison of the first simulation results revealed that in this setup the Hf-O distances were systematically larger than the Zr-O distances, which is in contrast to the experimental observations of Hf-bearing oxides or silicates having slightly smaller lattice constants than corresponding Zr-bearing crystals. We therefore tested

the Goedecker-Teter-Hutter pseudopotentials from Krack (2005) with semicore electrons for both Zr and Hf. The average Zr-O distance remained unchanged whereas the Hf-O distance decreased by about 0.05 Å and became shorter than the Zr-O distance. After having checked equivalence of the results from the two different types of pseudopotentials for the Zr-bearing fluids we continued to use Martins-Troullier type pseudopotentials but changed to Goedecker-Teter-Hutter pseudopotentials for the simulations of Hf-bearing fluids.

Partial radial distribution functions $g_{ij}(r)$ ($i, j$ =O, H, Zr, Hf, Na, Cl) and average coordination numbers were extracted from the calculated trajectories. Average coordination numbers were calculated by counting all relevant atom pairs with a distance smaller than the cutoff defined by the first minimum of the respective $g_{ij}(r)$. For Zr/Hf coordination by O and Cl atoms, cutoff radii of 3.0 Å and 3.5 Å were used, respectively (see Fig. 3). For O-H and H-Cl atom pairs we used cutoff distances of 1.27 Å and 1.60 Å. Further, we evaluated separately the Zr/Hf coordination by OH and $H_2O$ neighbors.

### *2.3. Theoretical XANES spectra*

Theoretical XANES spectra of the Zr $K-$edge and the Hf $L_3-$edge were calculated from the AIMD trajectories using the FEFF9 code (Rehr and Albers, 2000; Rehr et al., 2009). For each simulation run about 50 snapshots at equidistant time intervals (i.e. $\Delta t = 0.2$ ps for 10 ps total simulation time) were chosen and transformed into molecular clusters with the Zr or Hf atom positioned in the center. We checked that this sampling rate is sufficient to provide good averages for the theoretical XANES spectra. Hedin-Lundqvist muffin-tin type potentials were used for all calculations. The potentials were overlapped using the self-consistent field refinement loop. For this, a cluster radius of 4 Å was sufficient for the fluids. Full multiple scattering calculations were performed for cluster radii of 6 Å. In order to mimic the reduced broadening of the Zr K-edge XANES collected in partial fluorescence yield mode, the energy broadening of the calcu-

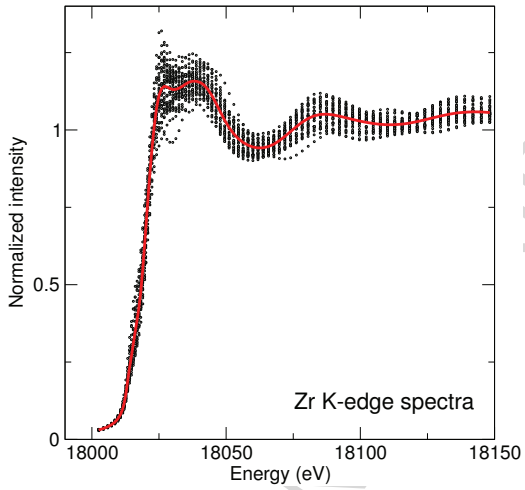


Figure 2: Individual (symbols) and average (line) XANES spectra for simulation run #Cl6b using the FEFF code.

lated spectra was decreased by setting the parameter for the imaginary potential to -1 for spectra of the fluids, which were measured in partial fluorescence mode using a high-resolution X-ray emission spectrometer and a Si(111) monochromator (c.f. Wilke et al. (2012)). Quadrupolar transitions have been included for all calculations, which is important to model the pre-edge feature of the Zr XANES. In case of Hf $L_3$-edge XANES the intrinsic energy broadening was used. The computed spectra of each trajectory were then averaged to obtain a final spectrum representative of the 10 ps simulation runs. To illustrate the spread of the individual spectra around the average spectrum, one example for simulation run #Cl6b is shown Fig. 2. In some of the Cl-bearing fluids, the number of Cl in the first coordination sphere of Zr or Hf changed in the course of the MD simulation. In those cases, only the part of the trajectory relevant to the complex of interest was considered in the averaging procedure.

As previously shown on crystalline model compounds (Wilke et al., 2012), the match between calculated and experimental Zr XANES spectra is very good. In the case of Hf, we have to note that measured and computed reference spectra for

a $HfO_2$ crystal show a systematic difference of about 4 eV between the relative positions of the first sharp XANES peak and the extended fine structure including the broad second maximum. In the case of the computed spectrum, the energy difference between the first and second maximum is about 4 eV too small, which is probably related to approximations made in the FEFF model calculations. A systematic error of similar size is expected in the $L_3$-edge spectra of the Hf-bearing solutions presented below, which should be kept in mind when comparing the respective spectra.

A second set of theoretical XANES calculations was performed using the FDMNES code (Joly, 2001; Bunau and Joly, 2009) to evaluate the consistency of the model spectra with calculations that go beyond the muffin-tin approximation. In FDMNES, the Schrödinger equation is solved by the finite difference method (FDM) within the local density approximation. A subset of nine snapshots for each AIMD run was used to obtain average spectra that show all relevant XANES features. The cluster radius was fixed to 3.35 Å, which is an optimized distance that includes the first coordination shell of Zr or Hf (see Fig. 3). The convergence of this choice was tested by a few calculations using an increased cluster radius of 4.5 Å. For the monomer species in solution, there was no significant difference between the computed spectra with different cutoff radii. The calculations of XANES spectra for clusters representing an eight-fold coordination environment similar to the high temperature phase of crystalline $ZrO_2$, a cluster radius of 4.0 Å was required to achieve convergence. Calculations included quadrupolar transitions. A core-hole broadening of 3 eV and a Fermi energy of -3 eV was used to match calculated Zr spectra to experiment in terms of position and broadening. For Hf, we used the respective values automatically determined within the FDMNES code.

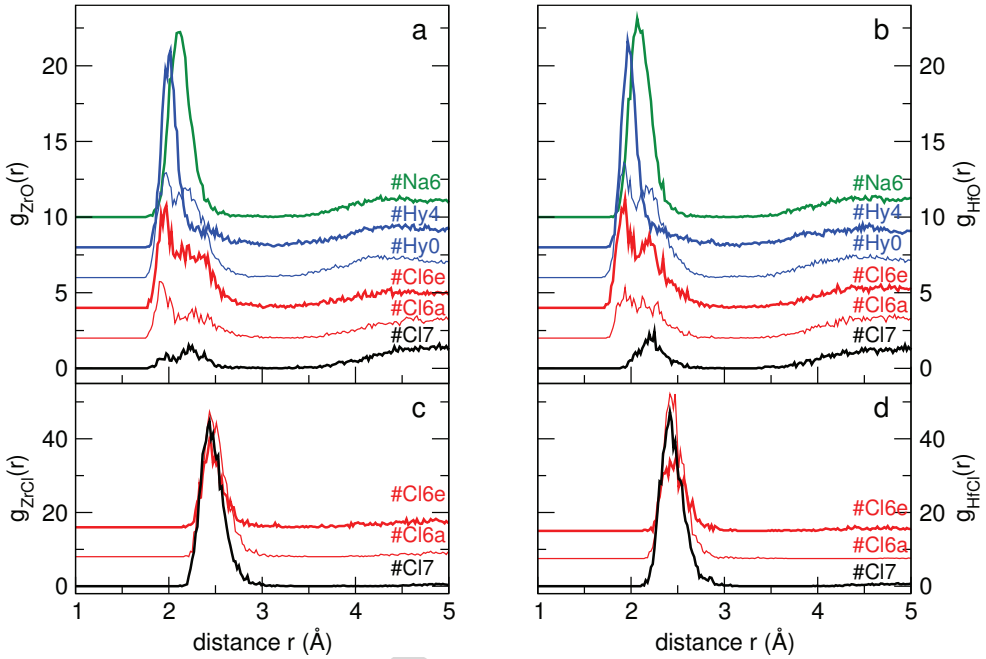


Figure 3: Radial distribution functions $g_{ij}(r)$ representing the distance $r$ between Zr/Hf and nearest neighbor anions: (a) Zr-O, (b) Hf-O, (c) Zr-Cl, (d) Hf-Cl. The double peak in $g_{ZrO}(r)$ and $g_{HfO}(r)$ arises from OH and $H_2O$ coexisting in the first coordination shell of Zr/Hf.

## 3. Results

### *3.1. Radial distribution functions*

We start to analyze the complexation of Zr and Hf in the investigated aqueous solutions by looking at the radial distribution functions, $g_{ij}(r)$, which describe the probability to find pairs of atoms of type $i$ and $j$ (here: $i, j$ =Zr, Hf, O, H, Na, Cl) separated by a distance $r$ normalized to the average partial number densities (Allen and Tildesley, 1987). Peak positions in $g_{ij}(r)$ are indicative of the most likely atomic distances whereas radial integration of $g_{ij}(r)$ allows to determine coordination numbers and average distances. Representative $g_{ij}(r)$s of Zr-O, Hf-O, Zr-Cl and Hf-Cl pairs are shown in Fig. 3. The first peak positions of $g_{ZrCl}(r)$ at about 2.45(2) Å and of $g_{HfCl}(r)$ at about 2.43(2) Å (see Table 2) are almost independent on composition. The same is true for the width and asymmetry of

the peak. Differences in absolute intensities are due to variations in the number of chlorine atoms in the first coordination shell of Zr/Hf (which will be presented below) and in the total number of Cl atoms in the simulation cell. Zr-Cl distances are slightly larger than Hf-Cl distances.

On the contrary, peak shapes and positions of $g_{ZrO}(r)$ and $g_{HfO}(r)$ vary significantly between different runs (see Fig. 3). Most of these radial distribution functions consist of a superposition of two features in the region of the first Zr/Hf coordination shell up to distances of about 3 Å. While the shorter distance is due to hydroxyl groups in the first coordination shell of Zr/Hf, the second peak arises from Zr/Hf-$OH_2$ neighbors. In the Zr-bearing solutions, the position of the first peak of $g_{ZrO}(r)$ shifts from about 1.92 Å in run #Cl6a to 2.10 Å in run #Na6. The first peak positions of $g_{HfO}(r)$ range from 1.90 Å in run #Cl6c to 2.07 Å in run #Na6 (Table 2). The broad Zr/Hf-O nearest neighbor distributions for $H_2O$ ligands have shallow maxima at about 2.2 to 2.3 Å.

### *3.2. Complexation in OH-bearing solutions*

Average coordination numbers and bond lengths of Zr/Hf complexes in OH-bearing solutions are summarized in Fig. 4 and Table 2. Generally, the final Zr/Hf coordination by oxygen is between 5.5 and 6.0. The only significant deviation from this trend is observed for run #Hy4 with an average of 5.3 (Zr) and 5.2 (Hf) oxygen neighbors. Run #Hy4 is characterized by charge neutral distorted Zr/Hf$(OH)_4$ tetrahedral unit to which one or two $H_2O$ molecules are added (and removed) frequently during the simulation.

In the simulations of OH-bearing solutions starting from initially more than 4 OH ligands (runs #Hy6, #Hy8, #Na5 and #Na6), the final Zr/Hf complexes consist of between five and six hydroxyl groups and only a very small fraction of transient $H_2O$ or pure O ($< 0.3$). Additional OH groups are released to the solvent. We could not find any appreciable difference in the Zr/Hf complexation between OH-bearing solutions with excess OH and negatively charged simulation

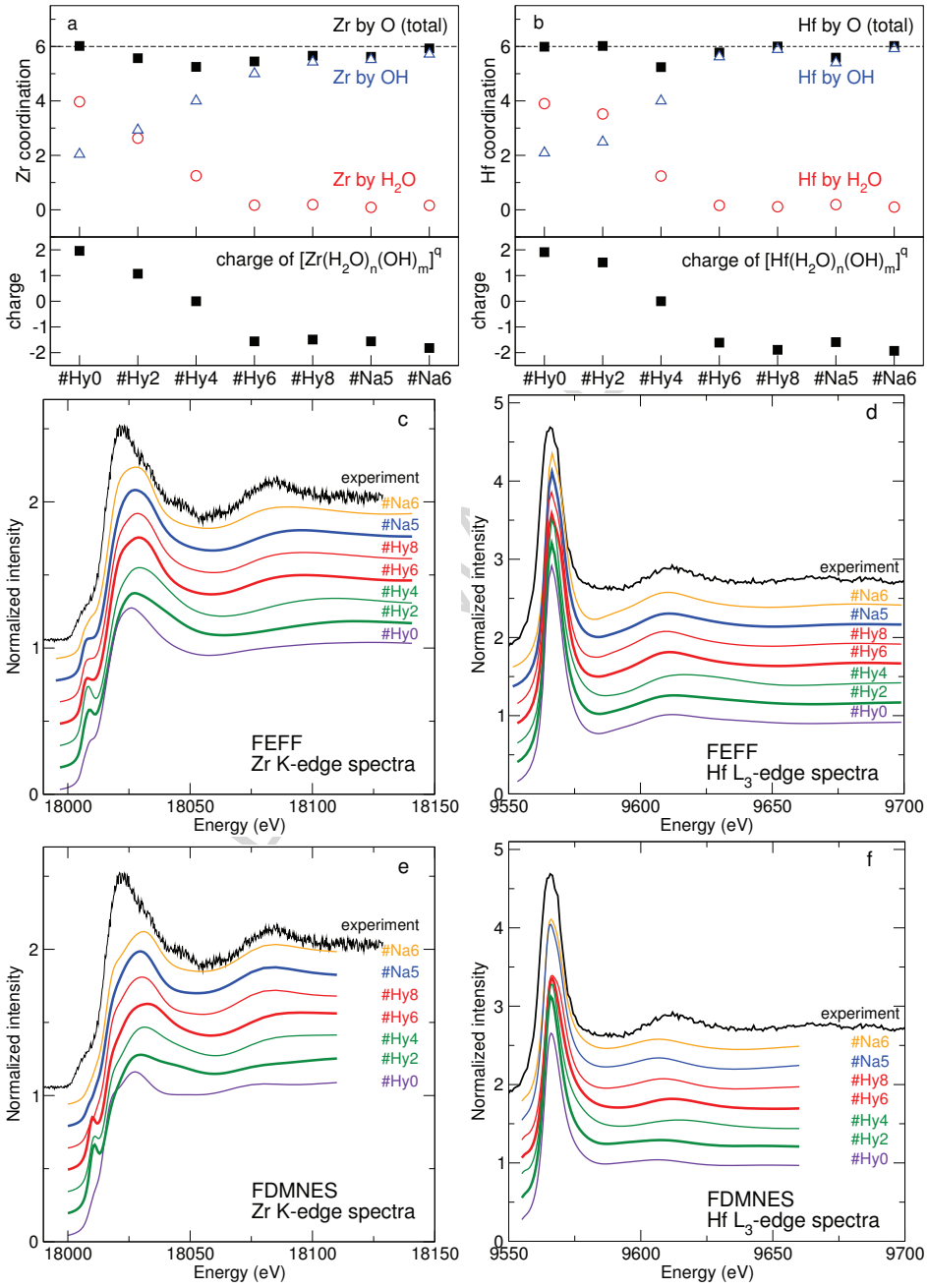


Figure 4: Average numbers of OH and $H_2O$ in the first coordination shells of Zr (a) and Hf (b), total coordination of Zr/Hf by oxygen, and formal charge of the respective Zr/Hf complex for OH-bearing fluids. Theoretical Zr K-edge (c,e) and Hf $L_3$-edge (d,f) XANES spectra of the different complexes in OH solutions sampled in runs #Hy0 to #Hy8, #Na5 and #Na6 compared to experimental spectra from Wilke et al. (2012, 2013). Experiments were performed for Zr in 6 wt% NaOH solution at $P = 0.79$ GPa, $T = 773$ K and Hf in 35 wt% NaOH solution at $P = 0.39$ GPa, $T = 773$ K.

Table 2: Average coordination numbers of Zr and Hf for the different runs. Values in brackets are average distances $r^{av}$ (in Å) from integration over the first coordination shell up to the cutoff distance used for evaluating the coordination number or peak positions $r^{max}$ (in Å) of the first maximum in the corresponding radial distribution function $g_{ij}(r)$.

| Run | Zr-O ($r^{av}$) | Zr-$OH_2$ | Zr-OH ($r^{max}$) | Zr-Cl ($r^{av}/r^{max}$) | Hf-O ($r^{av}$) | Hf-$OH_2$ | Hf-OH ($r^{max}$) | Hf-Cl ($r^{av}/r^{max}$) |
|---|---|---|---|---|---|---|---|---|
| #Hy0 | 6.0 (2.19) | 4.0 | 2.0 (1.96) | | 6.0 (2.16) | 3.9 | 2.1 (1.92) | |
| #Hy2 | 5.5 (2.17) | 2.6 | 2.9 (1.97) | | 6.0 (2.17) | 3.5 | 2.5 (1.93) | |
| #Hy4 | 5.3 (2.14) | 1.3 | 4.0 (2.00) | | 5.2 (2.11) | 1.2 | 4.0 (1.98) | |
| #Hy6 | 5.5 (2.12) | 0.2 | 5.3 (2.08)* | | 5.8 (2.11) | 0.2 | 5.6 (2.06)* | |
| #Hy8 | 5.6 (2.14) | 0.2 | 5.4 (2.08)* | | 6.0 (2.13) | 0.1 | 5.9 (2.08) | |
| #Na5 | 5.6 (2.13) | 0.1 | 5.5 (2.08)* | | 5.6 (2.11) | 0.2 | 5.4 (2.05)* | |
| #Na6 | 5.9 (2.16) | 0.2 | 5.7 (2.10)* | | 6.0 (2.13) | 0.1 | 5.9 (2.07)* | |
| #Cl9 | 0.0 | 0.0 | 0.0 | 6.0 (2.52/2.46) | 0.0 | 0.0 | 0.0 | 5.8 (2.49/2.41) |
| #Cl7 | 0.8 (2.25) | 0.6 | 0.2 | 5.0 (2.49/2.43) | 1.0 (2.26) | 0.9 | 0.1 | 5.0 (2.47/2.41) |
| #Cl6a | 2.1 (2.22) | 1.3 | 0.8 (1.92) | 4.0 (2.52/2.46) | 2.0 (2.17) | 1.3 | 0.7 (1.94) | 4.0 (2.48/2.43) |
| #Cl6b | 2.0 (2.18) | 1.2 | 0.8 (1.91) | 4.0 (2.53/2.46) | 2.0 (2.14) | 1.1 | 0.9 (1.94) | 4.0 (2.50/2.43) |
| #Cl6c | 3.0 (2.21) | 1.8 | 1.2 (1.94) | 3.0 (2.52/2.46) | 3.4 (2.25) | 2.4 | 1.0 (1.90) | 3.0 (2.50/2.44) |
| #Cl6d | 2.9 (2.22) | 1.9 | 1.0 (1.94) | 3.0 (2.48/2.46) | 2.8 (2.17) | 1.8 | 1.0 (1.92) | 3.0 (2.45/2.42) |
| #Cl6e | 4.2 (2.23) | 2.8 | 1.4 (1.95) | 2.0 (2.52/2.45) | 4.1 (2.17) | 2.6 | 1.5 (1.92) | 2.0 (2.50/2.43) |
| #Cl6f | 6.0 (2.18) | 3.6 | 2.4 (1.95) | 0.0 | 5.0 (2.14) | 3.0 | 2.0 (1.94) | 1.0 (2.51/2.45) |

*contain small fractions of Zr-O

cells (runs #Hy6 and #Hy8) and charge neutral NaOH solutions (runs #Na5 and #Na6).

For the hydroxide complexes with initially less than 4 $OH^-$ ligands (runs #Hy0 and #Hy2) significant hydrolysis takes place, which results in an increase of the number of hydroxyl groups in the first coordination shell of Zr/Hf and a reduction of the overall charge of the Zr/Hf complex. Due to proton transfer, the solvents contain in average 2.4 (#Hy0) and 0.6-1.1 (#Hy2) hydronium ($H_3O^+$) ions.

### *3.3. Complexation in chloride solutions*

Fig. 5 and Table 2 show average coordination numbers and bond lengths of Zr/Hf complexes in chloride solutions. As in the case of OH-bearing solutions, all of the AIMD runs evolve towards a 6-fold Zr/Hf coordination by anions (oxygen or chlorine). Due to the slow ligand exchange (about one per 10 ps) each MD run provides an average structure for a specific geometry and number of O and Cl in the first coordination shell (see Fig. 1). The ratio of OH to $H_2O$ neighbors fluctuates more quickly and reaches an average of around 0.5 in all chloride solution runs (Table 2). Consequently, the total formal charge of the hydroxy-chloride Zr and Hf complexes decreases monotonically with increasing number of coordinating Cl ions. As the simulation cells of the chloride solutions are charge neutral, the solvent has more negatively charged ions (Cl) in runs #Cl6e and #Cl6f, whereas $H_3O^+$ is the dominant ion in the solvent of all other runs #Cl6-9. In runs of the series #Cl6, the number of $H_3O^+$ in solution varies between 1.5 and 2.5. The respective numbers of $Cl^-$ and HCl increase from 0.5 (Hf-#Cl6a) to 3.4 (Zr-#Cl6f) and from 0.7 (Zr-#Cl6b) to 2.6 (Zr-#Cl6f). Due to the higher content of HCl, runs #Cl9 yield somewhat increased numbers of $H_3O^+$ (3.4 in Zr / 2.9 in Hf solution), HCl (2.0/2.5) and $Cl^-$ (1.0/0.5).

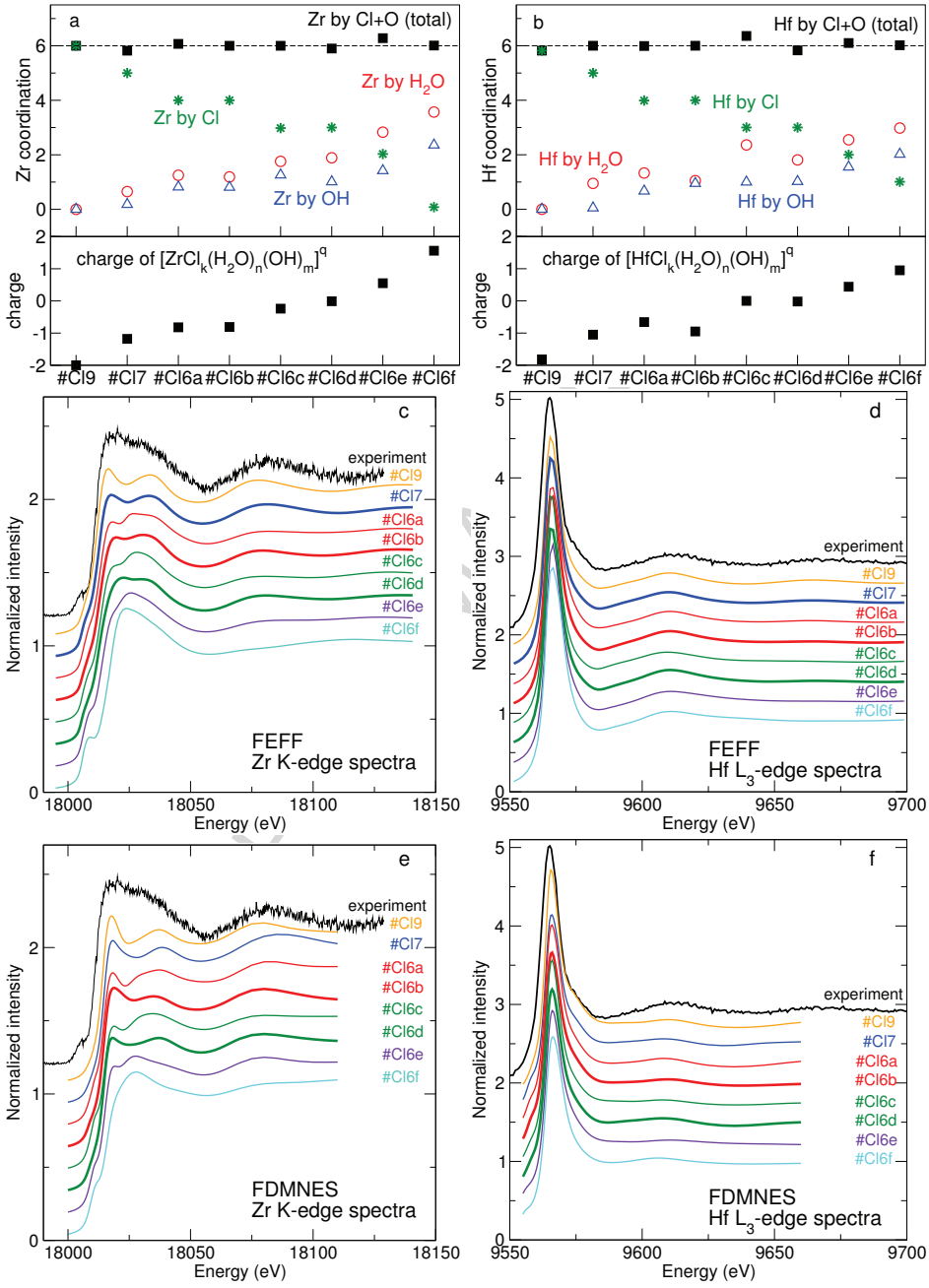


Figure 5: Average numbers of Cl, OH and $H_2O$ in the first coordination shell of Zr (a) and Hf (b), total coordination of Zr/Hf by Cl+O, and formal charge of the respective Zr/Hf complex for HCl fluids. Theoretical Zr K-edge (c,e) and Hf $L_3$-edge (d,f) XANES spectra of the different complexes in HCl solutions sampled in runs #Cl9, #Cl7 and #Cl6a-f compared to experimental spectra from Wilke et al. (2012, 2013). The experimental data were measured in 16 wt% HCl solution at $P = 1.37$ GPa, $T = 873$ K (Zr) and $P \sim 1$ GPa, $T = 773$ K (Hf).

### *3.4. Theoretical XANES spectra*

Theoretical XANES spectra are shown in Figs. 4c-f and 5c-f together with experimental data from Wilke et al. (2012) and Wilke et al. (2013). All computed spectra of the same edge are shifted by the same amount of energy to fit approximately the major peaks of the measured spectra.

Experimental Zr K-edge spectra are characterized by a small pre-edge feature at about 18008 eV, followed by a broad and asymmetric first maximum region between 18015 and 18050 eV, and a second maximum at around 18080 eV. The theoretical spectra of the OH-bearing fluids (Fig. 4c,e) show more or less pronounced pre-edge features and a similar first maximum region with a peak in the range between 18026 and 18032 eV, which is at somewhat larger energies than the experimental observation (18023 eV). The second broad maximum of the FEFF calculations varies between 18126 eV for run #Hy0 and 18090 eV for run #Na6. Some of the spectra from FDMNES calculations do not show a peak in this energy region. All of the theoretical spectra of runs #Hy0 to #Hy8, #Na5 and #Na6 show significant differences in both positions and line shape of the two major spectral regions compared to experiment. Zr K-edge spectra of the simulated chloride solutions are very sensitive to the specific coordination environment (Fig. 5c,e). With increasing number of Cl in the first coordination shell, the first maximum region becomes broader and eventually develops a double-peak structure for complexes with at least three Cl ligands. While corresponding theoretical spectra from FEFF and FDMNES calculations are slightly different in detail, the overall consistency is sufficient for a meaningful interpretation (see Discussion below).

Experimental Hf $L_3$-edge spectra are dominated by a sharp and intense absorption peak at 9565 eV with a shoulder on the high energy side at around 9576 eV. A second broad maximum is observed at 9613 eV. Theoretical spectra are similar to each other. They show small variations in the relative positions of the two major peaks and in the asymmetry of the major peak. The latter is somewhat

broader and more asymmetric in the case of chloride solutions, which is consistent with experiment (Figs. 4d,f and 5d,f). The systematic error in the calculation of the Hf $L_3$-edge spectra described in the methods section causes the position of the second broad maximum in the theoretical spectra shown in Figs. 4d,f and 5d,f to be shifted to slightly smaller energy (by about 4 eV) compared to the experimental spectra.

## 4. Discussion

The AIMD simulations presented here reveal a general preference of $Zr^{4+}$ and $Hf^{4+}$ monomer species in aqueous solutions for six-fold coordination at high pressure (about 1 GPa) and high temperature (1000 K) conditions. Anions of the first coordination shell form a more or less distorted octahedral environment (see e.g. Fig. 1). The distortion depends on the specific ligands. Zr/Hf-nearest neighbor anion distances increase in the order $OH^- < H_2O < Cl^-$. Further, Zr/Hf-OH distances increase with increasing number of OH in the first coordination shell whereas variations in the Zr/Hf-Cl distances with composition are much smaller (Table 2). Zr and Hf are usually considered geochemical twins and indeed we do not observe large differences in the complexation of these elements in aqueous solutions. It should be noted, however, that distances between $Hf^{4+}$ and nearest neighbor anions are systematically shorter by about 0.03(1) Å than distances between $Zr^{4+}$ and its neighbors. Also, the first peaks in the corresponding radial distribution functions seem to be slightly sharper for the Hf-bearing fluids (Fig. 3). Whether these small differences in the coordination environment have the capacity to fractionate Zr from Hf during fluid-rock interactions cannot be concluded from this study and needs to be addressed in the future.

Previous molecular dynamics simulation studies of HFSE were mainly concerned with the fully hydrated $(Ti,Zr,Hf)^{4+}(aq)$ complexes (van Sijl et al., 2010, 2011; Messner et al., 2011b,a). At ambient conditions, $Ti^{4+}$ is hydrated by five

$H_2O$ molecules van Sijl et al. (2010) whereas $[(Zr,Hf)(H_2O)_8]^{4+}$ complexes remained stable over a simulation period of 10 ps (Messner et al., 2011b,a). A change from ambient to supercritical conditions resulted in two significant changes in the complexation. First, hydrolysis reactions were observed in the first and second shell around $Ti^{4+}$ (van Sijl et al., 2010) and also mentioned to occur for $Zr^{4+}$ above 600 K (Messner et al., 2011b). In addition, the Ti coordination number changed from 5 at ambient conditions to 6 at 1000 K. In the present study, the simulations starting from the fully hydrated $Zr^{4+}$(aq) and $Hf^{4+}$ (run #Hy0) evolved towards a six-fold coordination of Zr/Hf by oxygen, of which about two belong to $OH^-$ groups and the remaining four to hydration $H_2O$. Thus, the major complexes of these simulations with charged simulation cells are $[(Zr,Hf)(OH)_2(H_2O)_4]^{2+}$. The mean coordination of first shell oxygen by hydrogen is about 1.7, which is similar to the value of 1.8 obtained for $Ti^{4+}$ (van Sijl et al., 2011). Thus, our AIMD study suggests that the complexation of $Zr^{4+}$ and $Hf^{4+}$ in strongly acidic environment at supercritical conditions is substantially different from the $[(Zr,Hf)(H_2O)_8]^{4+}$ speciation observed at ambient conditions and pH$< 0$.

Further insight into the most likely Zr and Hf complexation in concentrated supercritical HCl solutions is obtained by comparing theoretical XANES spectra of runs #Cl6, #Cl7 and #Cl6a-f to experimental data from Wilke et al. (2012, 2013) (see Fig. 5c-f). As the variations in the Hf $L_3$ spectra between different runs are rather small, we will focus the discussion on the Zr K-edge spectra. Nevertheless, there are two indicators in the Hf $L_3$ spectra that point to $Cl^-$ being the dominant ligands: a more pronounced shoulder on the high energy side of the intense first peak at about 9575 eV and the presence of a shallow maximum at about 9665 eV in the spectra of the Cl-rich species (e.g. #Cl7) as compared to the Cl-poor species (e.g. #Cl6f). The theoretical Zr K-edge spectra vary strongly between the different runs. The Zr complexation in #Cl6f is very similar to that in run #Hy0 already discussed above. Besides a small

increase in the number of $OH^-$ (which may still be within the statistical error), the main difference between these two runs is that the positive charge of $Zr^{4+}$ is compensated by a homogeneous charge background in run #Hy0 and by explicit $Cl^-$ ions in run #Cl6f. The similar XANES spectra of the respective Zr complexes are clearly different from the measured data, both in shape and positions of the main spectral features. From this observation we may conclude that a $Cl^-$-free coordination shell as reported at subcritical conditions does not exist in the supercritical HCl solutions studied experimentally, which contained 16 wt% HCl. Wilke et al. (2012) suggested a mixed oxychloride complex with 4 oxygen and 3 chlorine ligands. The AIMD simulations seem to provide a more realistic complex with only 6 Zr neighbors, of which 3 to 5 are $Cl^-$ ligands. In the real fluid, a distribution of different complexes may be present. According to the recent X-ray absorption spectroscopy study of Louvel et al. (2013), Zr complexation may change towards lower HCl concentration.

The charge neutral $[(Zr,Hf)(OH)_4(H_2O)_{1-2}]$ complex of run #Hy4 is a possible candidate for a monomeric Zr species in pure $H_2O$ solution at supercritical conditions. Its XANES spectra show strong shifts of the second broad peaks towards higher energies (to about 18110 eV for Zr and 9617 eV for Hf, see Fig. 4). However, it may be difficult to verify this hypothesis experimentally due to the very low concentration of zircon or hafnon in such neutral fluids. Compared to all other complexes discussed here and in the literature, $[(Zr,Hf)(OH)_4(H_2O)_{1-2}]$ has the lowest coordination number, which is closer to five than to six (Table 2).

In basic solutions, the number of $OH^-$ groups in the first coordination shell of $Zr^{4+}$ and $Hf^{4+}$ monomers is likely to increase above four. Such conditions are sampled in runs #Hy6, #Hy8, #Na5 and #Na6. The resulting coordination shells have 5.5 to 6.0 nearest neighbor oxygen atoms, which belong almost exclusively to $OH^-$ groups (Table 2). The theoretical XANES spectra derived from these four runs look very similar. However, in the case of the Zr K-edge the agreement with the experimental spectra in Fig. 4 is much less satisfactory than

for the chloride solutions. Peak positions of both principal spectral features are shifted to higher energy. Compared to reference compounds, the experimental NaOH spectrum is rather similar to that of $ZrO_2$ (baddeleyite). Therefore, Wilke et al. (2012) used a $ZrO_7$ cluster derived from a baddeleyite crystal as input structure for a FEFF calculation and obtained a spectrum that fitted better the first XANES peak but with a similar shift of the second broad peak as in the theoretical spectra presented here. To further elaborate on the importance of second neighbor contributions to the measured XANES spectra we performed short AIMD simulations of a tetragonal $ZrO_2$ crystal (the high temperature structure of $ZrO_2$) using a supercell with 48 atoms and setting $T = 1000$ K. Average XANES spectra from AIMD snapshots are shown in Fig. 6. Again, there is a general consistency between FEFF and FDMNES calculations, which suggests that the muffin-tin approximation is not a main cause for observed differences between experiment and simulation. The theoretical spectra reproduce the small peak at about 18045 eV in the experimental spectrum of the NaOH solution (slightly shifted to higher energies) if the Zr second neighbor shell is included in the cluster calculation. On the contrary, this peak is absent if only nearest neighbor oxygen atoms are considered. Together with the fact that our monomer simulations do not show any evidence for a Zr/Hf coordination larger than six and that all possible $OH^-/H_2O$ coordination shells do not fit the experimental spectrum sufficiently well, this strongly indicates the formation of polynuclear species in the experiment. The nature of such species and their apparent stability in aqueous fluids should be investigated in future studies.

The sensitivity of XANES spectroscopy to distinguish between different types of complexes with the same number of nearest-neighbor anions is nicely demonstrated by comparing the theoretical spectra of the Zr K-edge in Fig. 4c,e to experimental spectra of alkali silicate-bearing fluids measured, e.g., by Wilke et al. (2012) or Louvel et al. (2013). In all cases, $Zr^{4+}$ is sixfold coordinated by oxygen. The spectra of the alkali silicate fluids resemble closely spectra of Zr-bearing sil-

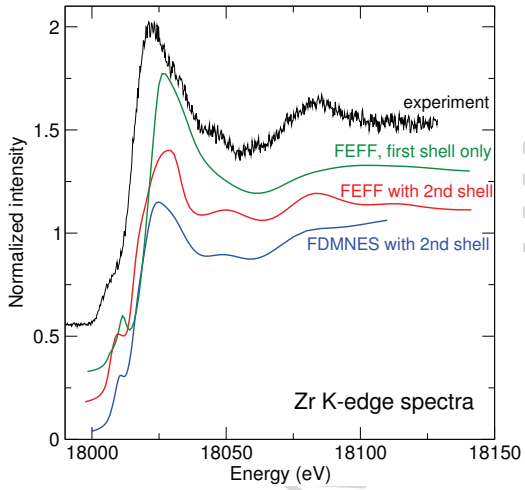


Figure 6: Theoretical XANES spectra for clusters with an eight-fold coordination environment similar to a tetragonal $ZrO_2$ crystal from snapshots of AIMD simulations at $T = 1000$ K. The small peak at about 18050 eV appears only if second Zr shell is considered in the calculations.

icates with octahedrally coordinated Zr (e.g. vlasovite) and show a much more pronounced splitting of the first XANES peak than the HCl solutions presented in Fig. 5c,e. Second neighbor cations (e.g. Si, Na but also H) and resulting distortions of the $ZrO_6$ octahedra apparently have a strong influence on details of the XANES spectra. These effects as well as thermal motions of the atoms are fully accounted for by using structural models from AIMD simulations. Extension of the present study of monomeric Zr and Hf species to oligomeric complexes is therefore needed to build reliable and complete speciation models for HFSE in supercritical fluids. Another challenge for future research will be to quantify the energetics of complex-forming reactions from first-principles simulations (see e.g. recent study by Mei et al. (2013)).

The results presented here cannot yet provide a fully comprehensive understanding of the HFSE complexation in natural supercritical fluids. However, the MD simulations together with the XAFS data provide strong evidence that HFSE complexation is strongly controlled by the fluid composition. As pointed out pre-

viously (e.g. (Manning, 2004)) the strongest control on the fluid composition in natural systems is likely provided by the rock matrix that buffers the chemical components dissolved in the fluid. The most concentrated Zr and Hf synthetic solutions, particularly those with extreme pH, are very unlikely to be responsible for mobilization of HFSE in natural settings. In addition, at supercritical conditions the low dielectric constant of solutions will not favor formation of the highly charged polymerized complexes known from low temperature solution chemistry. Likely candidates for very high solubilities of HFSE at high pressure and high temperature conditions are those solutions with dissolved alkali-aluminosilicate components because these can be provided through interaction with the adjacent rock matrix. Since the theoretical XANES spectra of Zr and Hf monomers presented here do not explain all features of the experimental XANES spectra, especially in the case of NaOH solutions at the Zr K-edge, the formation of other species, e.g. involving second neighbor cations such as other Zr/Hf, Si or Na, is likely and may be an important mechanism in natural systems.

## 5. Acknowledgments

The authors would like to thank three anonymous reviewers for their very useful comments and suggestions and the guest editor Carmen Sanchez-Valle for handling the manuscript. We gratefully acknowledge the computing time granted by the John von Neumann Institute for Computing (NIC) and provided on the supercomputers JUQUEEN and JUROPA at Jülich Supercomputing Centre (JSC). This work was supported by the German Research Foundation (DFG) under grants no. JA1469/4-1 and WI2000/5-1.

Aja, S. U., Wood, S. A., Williams-Jones, A. E., 1995. The aqueous geochemistry of Zr and the solubility of some Zr-bearing minerals. Appl. Geochem. 10, 603–620.

Allen, M. P., Tildesley, D. J., 1987. Computer simulations of liquids. Oxford University Press.

Antignano, A., Manning, C. E., 2008. Rutile solubility in $H_2O$, $H_2O$-$SiO_2$, and $H_2O$-$NaAlSi_3O_8$ fluids at 0.7-2.0 GPa and 700-1000 °C: Implications for mobility of nominally insoluble elements. Chem. Geol. 255, 283–293.

Audetat, A., Keppler, H., 2005. Solubility of rutile in subduction zone fluids, as determined by experiments in the hydrothermal diamond anvil cell. Earth Planet. Sci. Lett. 232, 393–402.

Bernini, D., Audetat, A., Dolejs, D., Keppler, H., 2013. Zircon solubility in aqueous fluids at high temperatures and pressures. Geochim. Cosmochim. Acta 119, 178–187.

Brendebach, B., Altmaier, M., Rothe, J., Neck, V., Denecke, M. A., 2007. EXAFS study of aqueous $Zr^{IV}$ and $Th^{IV}$ complexes in alkaline $CaCl_2$ solutions: $Ca_3[Zr(OH)_6]^{4+}$ and $Ca_4[Th(OH)_8]^{4+}$. Inorg. Chem. 46, 6804–6810.

Bunau, O., Joly, Y., 2009. Self-consistent aspects of x-ray absorption calculations. J. Phys.: Condens. Matter 21, 345501.

Cho, H.-R., Walther, C., Rothe, J., Neck, V., Denecke, M. A., Dardenne, K., Fanghänel, T., 2005. Combined LIBD and XAFS investigation of the formation and structure of Zr(IV) colloids. Anal. Bioanal. Chem. 383, 28–40.

Dempster, T. J., Hay, D. C., Bluck, B. J., 2004. Zircon growth in slate. Geology 32, 221–224.

Ekberg, C., Källvenius, G., Albinsson, Y., Brown, P. L., 2004. Studies on the hydrolytic behavior of zirconium(IV). J. Solution Chem. 33, 47–79.

Elliot, T., Plank, T., Zindler, A., White, W., Bourdon, B., 1997. Element transport from slab to volcanic front at the mariana arc. J. Geophys. Res. - Solid Earth 102, 14991–15019.

Ewing, R. C., Haaker, R. F., Lutze, W., 1982. Leachability of zircon as a function of alpha dose. In: Lutze, W. (Ed.), Scientific basis for radioactive waste management V. Elsevier, Amsterdam, pp. 389–397.

Hagfeldt, C., Kessler, V., Persson, I., 2004. Structure of the hydrated, hydrolysed and solvated zirconium(IV) and hafnium(IV) ions in water and aprotic oxygen donor solvents. A crystallographic, EXAFS spectroscopic and large angle x-ray scattering study. Dalton Trans. , 2142–2151.

Hayden, L. A., Manning, C. E., 2011. Rutile solubility in supercritical $NaAlSi_3O_8$-$H_2O$ fluids. Chem. Geol. 284, 74–81.

Jahn, S., Schmidt, C., 2010. Speciation in aqueous $MgSO_4$ fluids at high pressures and high temperatures from ab initio molecular dynamics and Raman spectroscopy. J. Phys. Chem. B 114, 15565–15572.

Jahn, S., Wunder, B., 2009. Lithium speciation in aqueous fluids at high P and T studied by ab initio molecular dynamics and consequences for Li-isotope fractionation between minerals and fluids. Geochim. Cosmochim. Acta 73, 5428–5434.

John, T., Klemd, R., Gao, J., Garbe-Schöneberg, C.-D., 2008. Trace-element mobilization in slabs due to non steady-state fluid-rock interaction: Constraints from an eclogite-facies transport vein in blueschist (Tienshan, China). Lithos 103, 1–24.

Joly, Y., 2001. X-ray absorption near-edge structure calculations beyond the muffin-tin approximation. Phys. Rev. B 63, 125120.

572 Kobayashi, T., Sasaki, T., Takagi, I., Moriyama, H., 2007. Solubility of zirco-
573 nium(IV) hydrous oxides. J. Nucl. Sci. Technol. 44, 90–94.

574 Kovalenko, N. I., Ryzhenko, B. N., 2009. Comparative study of the solubility of
575 zircon and baddeleyite. Geochem. Int. 47, 405–413.

576 Krack, M., 2005. Pseudopotentials for H to Kr optimized for gradient-corrected
577 exchange-correlation functionals. Theor. Chem. Acc. 114, 145–152.

578 Liati, A., Gebauer, D., 1999. Constraining prograde and retrograde P-T-t paths
579 of eocene HP rocks by SHRIMP dating of different zircon domains: inferred
580 rates of heating, burial, cooling and exhumation for central Rhodope, northern
581 Greece. Contrib. Mineral. Petrol. 1135, 340–354.

582 Liu, X., Lu, X., Wang, R., Zhou, H., 2012. First-principles molecular dynamics
583 study of stepwise hydrolysis reactions of $Y^{3+}$ cations. Chem. Geol. 334, 37–43.

584 Louvel, M., Sanchez-Valle, C., Malfait, W. J., Testemale, D., Hazemann, J.-L.,
585 2013. Zr complexation in high pressure fluids and silicate melts and implications
586 for the mobilization of HFSE in subduction zones. Geochim. Cosmochim. Acta
587 104, 281–299.

588 Manning, C. E., 2004. The chemistry of subduction-zone fluids. Earth Planet.
589 Sci. Lett. 223, 1–16.

590 Manning, C. E., Wilke, M., Schmidt, C., Cauzid, J., 2008. Rutile solubility in
591 albite-$H_2O$ and $Na_2Si_3O_7$-$H_2O$ at high temperatures and pressures by in-situ
592 synchrotron radiation micro-XRF. Earth Planet. Sci. Lett. 272, 730–737.

593 Marx, D., Hutter, J., 2000. Ab initio molecular dynamics: Theory and implemen-
594 tation. In: Grotendorst, J. (Ed.), Modern Methods and Algorithms of Quantum
595 Chemistry, Forschungszentrum Jülich, NIC Series. Vol. 1. pp. 301–449.

McCulloch, M. T., Gamble, J. A., 1991. Geochemical and geodynamical constraints on subduction zone magmatism. Earth Planet. Sci. Lett. 102, 358–374.

Mei, Y., Sherman, D. M., Liu, W., Brugger, J., 2013. Ab initio molecular dynamics simulation and free energy exploration of copper(I) complexation by chloride and bisulfide in hydrothermal fluids. Geochim. Cosmochim. Acta 102, 45–64.

Messner, C. B., Hofer, T. S., Randolf, B. R., Rode, B. M., 2011a. Computational study of the hafnium (IV) ion in aqueous solution. Chem. Phys. Lett. 501, 292–295.

Messner, C. B., Hofer, T. S., Randolf, B. R., Rode, B. M., 2011b. Structure and dynamics of the $Zr^{4+}$ ion in water. Phys. Chem. Chem. Phys. 13, 224–229.

Migdisov, A. A., Williams-Jones, A. E., van Hinsberg, V., Salvi, S., 2011. An experimental study of the solubility of baddeleyite ($ZrO_2$) in fluoride-bearing solutions at elevated temperature. Geochim. Cosmochim. Acta 75, 7426–7434.

Möller, A., O'Brien, P. J., Kennedy, A., Kröner, A., 2002. Polyphase zircon in ultrahigh-temperature granulites (Rogaland, SW Norway): Constraints for Pb diffusion in zircon. J. Metamorph. Geol. 20, 727–740.

Newton, R. C., Manning, C. E., Hanchar, J. M., Colasanti, C. V., 2010. Free energy of formation of zircon based on solubility measurements at high temperature and pressure. Am. Mineral. 95, 52–58.

Newton, R. C., Manning, C. E., Hanchar, J. M., Finch, R. J., 2005. Gibbs free energy of formation of zircon from measurement of of solubility in $H_2O$. J. Am. Ceram. Soc. 88, 1854–1858.

Nosé, S., 1984. A molecular dynamics method for simulations in the canonical ensemble. Mol. Phys. 52, 255–268.

Perdew, J. P., Burke, K., Ernzerhof, M., 1996. Generalized gradient approximation made simple. Phys. Rev. Lett. 77, 3865–3868.

Perfit, M. R., Gust, D. A., Bence, A. E., Arculus, R. J., Taylor, S. R., 1980. Chemical characteristics of island-arc basalts: Implications for mantle sources. Chem. Geol. 30, 227–256.

Philippot, P., Selverstone, J., 1991. Trace-element-rich brines in eclogite veins: implications for fluid composition and transport during subduction. Contrib. Mineral. Petrol. 106, 417–430.

Qiu, L., Guzonas, D. A., Webb, D. G., 2009. Zirconium dioxide solubility in high temperature aqueous solutions. J. Solution Chem. 38, 857–867.

Rao, N., Holerca, M. N., Klein, M. L., Pophristic, V., 2007. Computational study of the $Zr^{4+}$ tetranuclear polymer $[Zr_4(OH)_8(H_2O)_{16}]^{8+}$. J. Phys. Chem. A 111, 11395–11399.

Rapp, J. F., Klemme, S., Butler, I. B., Harley, S. L., 2010. Extremely high solubility of rutile in chloride and fluoride-bearing metamorphic fluids: An experimental investigation. Geology 38, 323–326.

Rehr, J. J., Albers, R. C., 2000. Theoretical approaches to x-ray absorption fine structure. Rev. Mod. Phys. 72, 621–654.

Rehr, J. J., Kas, J. J., Prange, M. P., Sorini, A. P., Takimoto, Y., Vila, F. D., 2009. Ab initio theory and calculations of x-ray spectra. C. R. Phys. 10, 548–559.

Ryzhenko, B. N., Kovalenko, N. I., Prisyagina, N. I., Starshinova, N. P., Krupskaya, V. V., 2008. Experimental determination of zirconium speciation in hydrothermal solutions. Geochem. Int. 46, 328–339.

645 Schmidt, C., Rickers, K., Wirth, R., Nasdala, L., Hanchar, J. M., 2006. Low-
646 temperature zr mobility: An in situ synchrotron-radiation XRF study of the
647 effect of radiation damage in zircon on the element release in $H_2O$ + HCl ±
648 $SiO_2$ fluids. Am. Mineral. 91, 1211–1215.

649 Sherman, D. M., 2010. Metal complexation and ion association in hydrothermal
650 fluids: insights from quantum chemistry and molecular dynamics. Geofluids
651 10, 41–57.

652 Singhal, A., Toth, L. M., Lin, J. S., Affholter, K., 1996. Zirconium(IV)
653 tetramer/octamer hydrolysis equilibrium in aqueous hydrochloric acid solu-
654 tion. J. Am. Chem. Soc. 118, 11529–11534.

655 Tole, M. P., 1985. The kinetics of dissolution of zircon ($ZrSiO_4$). Geochim. Cos-
656 mochim. Acta 49, 453–458.

657 Tropper, P., Manning, C. E., 2005. Very low solubility of rutile in $H_2O$ at high
658 pressure and temperature, and its implications for Ti mobility in subduction
659 zones. Am. Mineral. 90, 502–505.

660 van Sijl, J., Allan, N. L., Davies, G. R., van Westrenen, W., 2010. Titanium in
661 subduction zone fluids: First insights from ab initio molecular metadynamics
662 simulations. Geochim. Cosmochim. Acta 74, 2797–2810.

663 van Sijl, J., Allan, N. L., Davies, G. R., van Westrenen, W., 2011. Solvation of
664 Ti(IV) in aqueous solution under ambient and supercritical conditions. Phys.
665 Chem. Chem. Phys. 13, 7371–7377.

666 Veyland, A., Dupont, L., Pierrard, J.-C., Rimbault, J., Aplincourt, M., 1998.
667 Thermodynamic stability of zirconium(IV) complexes with hydroxy ions. Eur.
668 J. Inorg. Chem. , 1765–1770.

669 Wagner, W., Pruss, A., 2002. The IAPWS formulation 1995 for the thermody-
670 namic properties of ordinary water substance for general and scientific use. J.
671 Phys. Chem. Ref. Data 31, 387–535.

672 Watenphul, A., Schmidt, C., Jahn, S., 2014. Cr(III) solubility in aqueous fluids
673 at high pressures and temperatures. Geochim. Cosmochim. Acta 126, 212–227.

674 Weingärtner, H., Franck, E. U., 2005. Supercritical water as a solvent. Angew.
675 Chem. Int. Ed. 44, 2672–2692.

676 Wilke, M., Jahn, S., Schmidt, C., Dubrail, J., Appel, K., Borchert, M., Kvash-
677 nina, K., Pascarelli, S., Manning, C. E., 2013. Insights from x-ray absorp-
678 tion/fluorescence spectroscopy and ab-initio molecular dynamics on concentra-
679 tion and complexation of Zr and Hf in aqueous fluids at high pressure and
680 temperature. J. Phys.: Conf. Ser. 430, 012122.

681 Wilke, M., Schmidt, C., Dubrail, J., Appel, K., Borchert, M., Kvashnina, K.,
682 Manning, C. E., 2012. Zircon solubility and zirconium complexation in $H_2O$ +
683 $Na_2O$ + $SiO_2$ ± $Al_2O_3$ fluids at high pressure and temperature. Earth Planet.
684 Sci. Lett. 349-350, 15–25.

**Highlights**

- ab initio molecular dynamics simulation of supercritical Zr and Hf solutions
- complexation strongly dependent on fluid composition
- dominant chloride species different from ambient conditions
- theoretical XANES spectra in good agreement with experiment